Ado Jorio · Mildred S. Dresselhaus
Gene Dresselhaus *Editors*

TOPICS IN APPLIED PHYSICS 111

# Carbon Nanotubes

## Advanced Topics in the Synthesis, Structure, Properties and Applications

Springer

# Ultrafast Spectroscopy of Carbon Nanotubes

Ying-Zhong Ma[1,2], Tobias Hertel[3], Zeev Valy Vardeny[4], Graham R. Fleming[1,2], and Leonas Valkunas[5,6]

[1] Department of Chemistry, University of California, Berkeley, CA 94720-1460, USA
yzma@berkeley.edu
[2] Physical Biosciences Division, Lawrence Berkeley National Laboratory, Berkeley, CA 94720-1460, USA
GRFleming@lbl.gov
[3] Department of Physics and Astronomy, Vanderbilt University, Nashville, TN 37235, USA
tobias.hertel@vanderbilt.edu
[4] Department of Physics, University of Utah, 1400 East 115 South, Salt Lake City, Utah 84112, USA
val@nova.physics.utah.edu
[5] Institute of Physics, Vilnius University, Savanoriu Ave. 231, 02300 Vilnius, Lithuania
Leonas.Valkunas@ff.vu.lt
[6] Theoretical Physics Department, Faculty of Physics of Vilnius University, Sauletekio Ave. 9, build. 3, 10222 Vilnius, Lithuania

**Abstract.** Time-domain spectroscopic studies provide a unique perspective on the materials properties and the microscopic processes underlying them in carbon nanotubes. Ultrafast spectroscopy is used to study the dynamics and kinetics of scattering and relaxation processes from the femtosecond ($1\,\mathrm{fs} \equiv 10^{-15}\,\mathrm{s}$) to the picosecond timescale. This provides crucial information on carrier and exciton dynamics that underpin a variety of potential applications of carbon nanotubes, from their use as current-carrying quantum wires, through light-emitting or detecting nanodevices, to their use in light-harvesting technologies and photovoltaics. Background information on the ultrafast spectroscopic techniques of greatest applicability to nanotubes is also provided.

## 1 Introduction[1]

The remarkable advances in the generation and characterization of tunable, intense, ultrashort light pulses and in optoelectronic detection have made ultrafast spectroscopy a powerful tool for studies of electronic and vibrational excitations in complex systems. By exciting a given system perturbatively it is now possible to follow various dynamical processes by means of diverse techniques with high spectral and temporal resolution. Studies of the excitation dynamics in carbon nanotubes began only a few years ago and have been almost entirely focused on the population relaxation of electronic excited

[1] Ying-Zhong Ma and Tobias Hertel have contributed equally to this contribution.

A. Jorio, G. Dresselhaus, M. S. Dresselhaus (Eds.): Carbon Nanotubes,
Topics Appl. Physics **111**, 321–352 (2008)

states. Despite its infancy, this rapidly developing field has been particularly fruitful for the identification of several fundamental properties and has seen a continuous emergence of fascinating discoveries. In this contribution, we will review the major advances in this field.

This review begins in Sect. 2 with an introduction to the experimental and theoretical background for nonlinear optical spectroscopy. We will first in Sect. 2.1 introduce typical instrumentation for ultrafast spectroscopy. Subsequently, we will describe briefly in Sect. 2.2 some of the fundamentals of nonlinear optics and spectroscopy with an emphasis on connecting the physical quantities of interest to the experimental observables. In Sect. 3, we will discuss pioneering work on metallic nanotubes, which represents the historic origins of this exciting field. This is followed by an overview of exciton dynamics in semiconducting nanotubes in Sect. 4. Following a general discussion of exciton dynamics, we will review separately studies conducted under low and high excitation intensities. In Sect. 5, we will discuss some similarities between semiconducting nanotubes and $\pi$-conjugated polymers. The review concludes in Sect. 6 with a summary and an outlook for future directions. In addition to the contributions to this book cited above, the authors also note a discussion of measurements of the dynamics of radial breathing and the G-band Raman-active modes in the contribution by Kono et al. as measured by impulsive excitation techniques.

## 2 Background

### 2.1 Instrumentation for Ultrafast Spectroscopy

The key component of any ultrafast spectroscopic setup is a light source that can deliver femtosecond pulses at desired wavelengths. Today's Ti:sapphire mode-locked laser technology has become a standard for such applications and is commercially available, allowing routine generation of sub-100 fs pulses near 800 nm with pulse energies from a few nJ to over 1 mJ [1] at repetition rates from 80 MHz to 1 kHz, respectively. Frequency-conversion technology allows extension of the Ti:sapphire output from the near-ultraviolet (UV), through the visible to the near- and mid-infrared regions [1, 2] (see Fig. 1). This provides unique opportunities for experimental studies of ultrafast dynamics in single-walled carbon nanotubes (SWNTs) and other systems.

The techniques used for ultrafast optical studies can coarsely be divided into directly time-resolved schemes that employ fast detectors and into gated- or pump-probe detection schemes that can be performed with slow detectors.

Transient or synchronized differential absorption spectroscopy is one specific type of a variety of femtosecond time-resolved pump-probe spectroscopies, wherein an initial pump pulse excites a sample, and the resulting change of sample absorbance at the frequency $\omega$ is measured by a probe pulse at a specific time delay $\Delta t$ [3–5]. The resulting differential absorbance

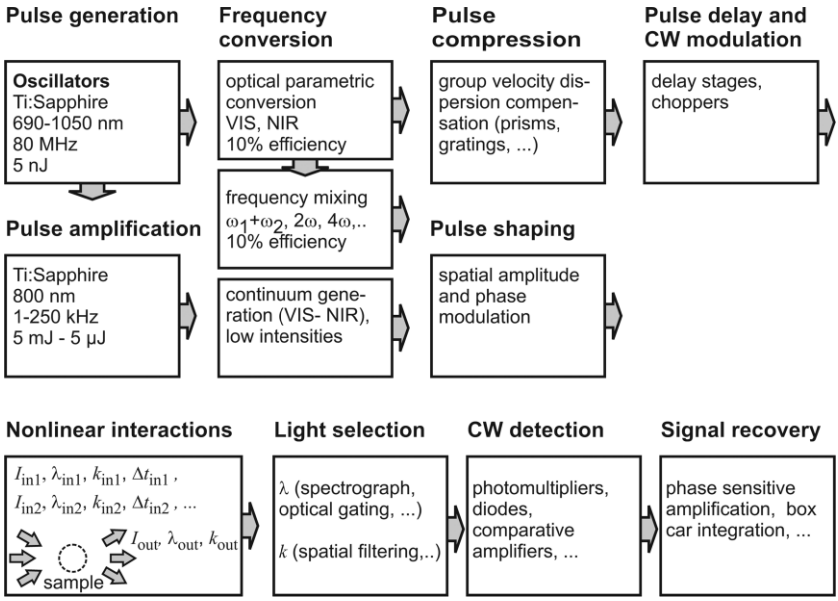


**Fig. 1.** Block diagram of the components of a generic time-resolved experiment. One or more components from each stage may be combined in a specific setup. *Numbers* for frequencies and pulse energies reflect approximate values

$\Delta\alpha(\omega, \Delta t)$ is then recorded as a function of the time delay between the pump and probe pulses, which is controlled by an optical delay line. The intensity of the probe and/or reference beams may be detected spectrally integrated or frequency resolved by a single-channel photodiode or by multichannel detection using CCD cameras or diode arrays. Phase-sensitive amplification is frequently used in conjunction with single-channel detection schemes to enhance the sensitivity down to $10^{-6}$. Different variants of this technique are distinguished from one another based on the specific choice of the frequencies of the pump and probe beams ($\omega_{\mathrm{p}}$ and $\omega_{\mathrm{pr}}$), their propagation direction ($k_{\mathrm{p}}$ and $k_{\mathrm{pr}}$, which can be collinear or skewed), and their respective polarizations ($\epsilon_{\mathrm{p}}$ and $\epsilon_{\mathrm{pr}}$). The resulting schemes are referred to as nondegenerate or degenerate, interferometric or polarization anisotropy pump-probe spectroscopy, to name only the most commonly used pump-probe varieties.

Another pump-probe detection scheme is time-resolved photoemission (TRPE) where a visible pump pulse creates a nonequilibrium electron distribution and a UV probe pulse monitors the state of the electronic system by photoemission of electrons from the sample. Energy-selective detection of photoemitted electrons can be realized using hemispherical analyzers or by the time-of-flight technique. The photoelectron intensity within a certain energy interval is then recorded as a function of $\Delta t$, allowing the extraction of dynamical information on changes of the nonequilibrium electron distribu-

tion $f_{\mathrm{ne}}$ [6–11]. Due to the small mean free path of low-energy photoelectrons, this technique is mostly limited to the exploration of carrier dynamics in the vicinity of vacuum/solid interfaces.

Time-integrating detectors can also be used to measure the ultrafast dynamics of photoluminescence (PL) decay by means of optical gating techniques, such as Kerr gating or fluorescence upconversion [4, 12–15]. The latter technique involves mixing of the fluorescence signal with an intense gate pulse in a nonlinear crystal. The resulting sum-frequency signal is measured as a function of the time delay between an ultrafast pump pulse used for the excitation and the gate pulse. The emission wavelength to be probed is selected simply by means of the angle at which the nonlinear crystal is aligned with respect to the fluorescence and gate beams. The upconverted signal is usually detected by a photomultiplier connected to a photon counter.

The pump-probe and gating techniques described above typically allow one to achieve sub-100 fs time resolution but they can occasionally also reach 10 fs or less. Direct measurements of time-resolved fluorescence with a time resolution of up to about 10 ps, on the other hand, are routinely achievable with fast detectors, e.g., photomultipliers (PMs), avalanche photodiodes (APDs) or streak cameras. Time-correlated single photon counting (TCSPC) for example, refers to the measurement of fluorescence signals using single photon detectors, such as APDs or PMs in combination with fast time-to-amplitude converters that can achieve an overall time resolution of a few tens of picoseconds [12, 16]. The high detection sensitivity of TCSPC, moreover, allows the study of individual SWNTs [17]. A time resolution of 1 ps can be achieved by some streak cameras, which enable simultaneous detection of both spectral and temporal information [12, 18].

### 2.2 Basics of Nonlinear Optics

The basis of practically all time-resolved pump-probe techniques is the nonlinear response of a medium to excitation with light. Light–matter interactions result in frequency-dependent changes of the radiation field as a consequence of elastic or inelastic scattering and/or absorption by the illuminated system. The resulting polarization $P$ of the dielectric medium is coupled to the external transverse electromagnetic field $E(\boldsymbol{r}, t)$ according to the wave equation [19]:

$$\Delta E(\boldsymbol{r}, t) - \frac{1}{c^2}\frac{\partial^2}{\partial t^2}E(\boldsymbol{r}, t) = -\frac{4\pi}{c^2}\frac{\partial^2}{\partial t^2}P(\boldsymbol{r}, t)\,, \tag{1}$$

where $c$ is the speed of light. Generally, internal electric fields between and within atoms are on the order of $10^{10}$ V/cm and are strong in comparison with even the most intense laser fields used for spectroscopic applications [20, 21]. To distinguish between linear ($P^{(1)}$) and nonlinear ($P_{\mathrm{NL}}$) effects in the re-

sponse of the polarization, one commonly expands $P$ in powers of the electric field strength $E(\boldsymbol{r},t)$:

$$P(\boldsymbol{r},t) = P^{(1)}(\boldsymbol{r},t) + P^{(2)}(\boldsymbol{r},t) + P^{(3)}(\boldsymbol{r},t) + \cdots \equiv P^{(1)}(\boldsymbol{r},t) + P_{\mathrm{NL}}(\boldsymbol{r},t)\,. \quad (2)$$

The nonlinear polarization $P_{\mathrm{NL}}$ carries the complete information needed for the description of any nonlinear optical process. To calculate $P_{\mathrm{NL}}$, one needs to solve equations that describe the microscopic light–matter interactions. A semiclassical procedure is usually employed: the external field is treated classically, whereas the polarization of the system is calculated quantum mechanically. Thus, the system is characterized by the Hamiltonian $H_0$ and its interaction with the external electromagnetic field is described by the term [22]:

$$V_{\mathrm{int}} = -\boldsymbol{\mu}E(t)\,, \quad (3)$$

where $\boldsymbol{\mu}$ is the dipole moment of the system and $E(t)$ is the time-dependent electric-field component of the incident light. The evolution of the system perturbed by an external electromagnetic field can be determined by solving the Liouville–von Neumann equation [23]:

$$\frac{\partial\rho}{\partial t} = \frac{1}{i\hbar}[H_0 + V_{\mathrm{int}}, \rho] + \dot{\rho}_{\mathrm{diss}}\,, \quad (4)$$

where $\rho$ is the density matrix of the system, $[H_0 + V_{\mathrm{int}}, \rho]$ designates the commutator between the Hamiltonian of the unperturbed system plus the interaction with the electromagnetic field $V_{\mathrm{int}}$ and the density matrix $\rho$, and $\dot{\rho}_{\mathrm{diss}}$ refers to dissipative processes, such as radiative and nonradiative decay. If the electric field is small compared to the internal fields of the system, we can expand the density matrix operator $\rho(t)$ in powers of the electric field:

$$\rho(t) = \rho^{(0)}(t) + \rho^{(1)}(t) + \rho^{(2)}(t) + \cdots\,, \quad (5)$$

where $\rho^{(n)}(t)$ is the $n$th-order contribution. The corresponding polarization $P^{(n)}$ is given by the expectation value of the dipole-moment operator $P^{(n)}(t) = \langle\boldsymbol{\mu}|\rho^{(n)}(t)\rangle$. Introducing the nonlinear response function $S^{(n)}$ the $n$th-order polarization $P^{(n)}$ can be written as:

$$P^{(n)}(t) = \int_0^\infty \mathrm{d}t_n \int_0^\infty \mathrm{d}t_{n-1} \cdots \int_0^\infty \mathrm{d}t_1 S^{(n)}(t_n, t_{n-1}, \ldots, t_1) \times E(t-t_n)E(t-t_n-t_{n-1})\cdots E(t-t_n-t_{n-1}-\cdots-t_1)\,. \quad (6)$$

The derivation of this equation and the functional forms of the first, second- and third-order response functions can be found in the literature (see, for instance, [22]). For centrosymmetric systems or isotropic media,

all even-order polarization terms vanish, and therefore the lowest term in $P_{\mathrm{NL}}$ is $P^{(3)}$. The third-order polarization dominates most nonlinear spectroscopies, such as photon-echo, transient grating, pump-probe, Raman scattering, two-dimensional (2D) electronic spectroscopy, etc. [22, 24]. The pump-probe signal, for example, is given by [25]:

$$I_{\mathrm{PP}}(\omega_{\mathrm{pr}}, \Delta t) = 2\omega_{\mathrm{pr}}\mathrm{Im}\int_{-\infty}^{+\infty} \mathrm{d}t' E_{\mathrm{pr}}(t') P^{(3)^*}(0, \Delta t, t')\,, \tag{7}$$

where $\omega_{\mathrm{pr}}$ and $E_{\mathrm{pr}}$ are the carrier frequency and the electric-field envelope of the probe pulse, respectively, and $\Delta t$ denotes the time delay between the pump and probe pulses. Here, $E_{\mathrm{pr}}$ also acts as a local oscillator, and a significantly amplified signal is achieved through intrinsic optical heterodyne detection (OHD) by coherently mixing it with a weak signal field along the same direction. An advantage of OHD is that the signal is linear with the third-order polarization $P^{(3)}$. Since $P^{(3)}$ is proportional to the third power of the electric field, the pump-probe signal should be linearly dependent on the intensity of the pump and probe pulses.

If the timescales on which the charge- and energy-transfer processes occur are large with respect to the dephasing times of the system, however, the optical transients can be described semiclassically using the frequency-dependent absorption coefficient $\alpha(\omega)$:

$$\alpha(\omega) = \frac{\omega\epsilon_2(\omega)}{n(\omega)c}\,. \tag{8}$$

Changes of $\alpha$ in transient spectra can thus be traced to changes of $\epsilon_2$, the imaginary part of the dielectric function, which can be written as:

$$\epsilon_2(\omega) = \frac{2\pi e}{m_e\omega}\sum_{\mathrm{i,f}}\sum_{k}|M_{\mathrm{fi}}|^2\rho_{\mathrm{ii}}(1-\rho_{\mathrm{ff}})\delta(E_{\mathrm{f}}(k) - E_{\mathrm{i}}(k) - \hbar\omega)\,, \tag{9}$$

in which the summation runs over all initial i and final f states with momentum $k$, and over the corresponding state populations $\rho_{\mathrm{ii}}$ and $\rho_{\mathrm{ff}}$ that are coupled to the electromagnetic field by the transition dipole matrix element $M_{\mathrm{fi}}$. For transitions between two specific states $|1\rangle$ and $|2\rangle$ the change of the absorption coefficient measured in the transient spectra can then be related to:

$$\Delta\epsilon_2(\omega) = \frac{2\pi e}{m_e\omega}|M_{21}|^2[(1-\rho_{22})\Delta\rho_{11} - \rho_{11}\Delta\rho_{22}]\,, \tag{10}$$

where $\Delta\rho_{11}$ and $\Delta\rho_{22}$ denote the population changes. Combining (8) and (10) for small excitation densities $\rho_{22} \ll \rho_{11}$, we finally obtain the semiclassical expression for the transient absorption signal in the incoherent limit:

$$\Delta\alpha(\omega) = \frac{2\pi e}{m_e n(\omega)c}|M_{21}|^2[\Delta\rho_{11} - \Delta\rho_{22}]\,. \tag{11}$$

This incoherent limit is frequently used as a basis for the interpretation of optical transients.

## 3 Metallic Tubes

The electron–phonon (el–ph) interaction in metallic carbon nanotubes (see also the contribution by Saito et al.) plays a key role for several critical materials properties such as the temperature dependence of the electrical conductivity [26], their thermoelectric power [27], and possibly superconductivity [28]. Electron–phonon interactions can also induce subtle changes in the electronic band structure and open a small bandgap at the Fermi level of metallic SWNTs [29, 30]. Metallic SWNTs have, furthermore, been found to carry exceedingly large current densities of $10^7$–$10^8\,\mathrm{Acm}^{-2}$ at room temperature without suffering current-induced damage [31, 32]. This is indicative of weak el–ph interactions that facilitate ballistic electron transport over long distances. We discuss here the first experiment studying carrier dynamics in metallic SWNTs using TRPE spectroscopy [33], which allows study of the carrier dynamics in the vicinity of the Fermi level in real time. For a brief description of the TRPE technique see Sect. 2.1.

Differential photoelectron spectra are recorded as a function of pump-probe delay. The kinetic energy of the photoemitted electrons here allows the observed transient spectra to be identified with the carrier dynamics in metallic tubes because semiconducting tubes do not contribute to the density of states near the Fermi level. The initial electron-gas thermalization is found to proceed on a 200 fs timescale. The evolution of the effective electron gas temperature from the moment of excitation up to time delays of 6 ps is shown in Fig. 2. The observed electron-gas cooling can here solely be attributed to the coupling of electronic and lattice degrees of freedom. The coupling of a thermalized electron distribution with temperature $T_\mathrm{e}$ to a lattice at temperature $T_\mathrm{l}$ is generally described by the so-called two-temperature model of *Anisimov* et al. [34]:

$$C_\mathrm{e}\frac{\mathrm{d}T_\mathrm{e}}{\mathrm{d}t} = \nabla(\kappa\nabla T_\mathrm{e}) - H(T_\mathrm{e}, T_\mathrm{l}) + S(t)\,, \tag{12}$$

$$C_\mathrm{l}\frac{\mathrm{d}T_\mathrm{l}}{\mathrm{d}t} = H(T_\mathrm{e}, T_\mathrm{l})\,, \tag{13}$$

where $C_\mathrm{e}$ and $C_\mathrm{l}$ refer to the electron and lattice specific heat capacities, respectively, $\kappa$ is the electronic heat diffusion coefficient, $S(t)$ is the source term describing the energy deposited in the electronic system by the pump pulse and $H(T_\mathrm{e}, T_\mathrm{l})$ is the coupling term that describes the coupling strength between electronic and lattice degrees of freedom. In the low-temperature limit with electronic temperatures similar to or smaller than the Debye temperature $\Theta_\mathrm{D}$, the coupling term can be written as [35]:

$$H(T_\mathrm{e}, T_\mathrm{l}) = \frac{144\zeta(5)k_\mathrm{B}\gamma}{\pi\hbar}\frac{\lambda}{\Theta_\mathrm{D}^2}(T_\mathrm{e}^5 - T_\mathrm{l}^5)\,, \tag{14}$$

where $\zeta(5) = 1.0369\ldots$ is the Riemann zeta function, $\gamma$ is the electronic heat capacity coefficient and $\lambda$ is the el–ph mass enhancement factor [36]. By

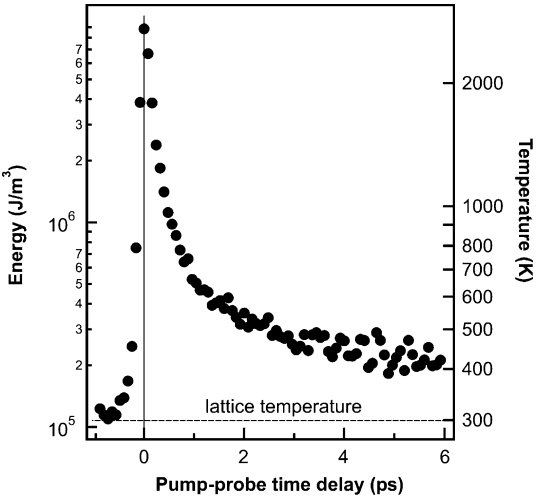


**Fig. 2.** Kinetic energy of the photoemitted electrons vs. time delay shows the laser heating and successive cooling back to the lattice temperature as driven by the electron–phonon coupling. (From [7])

assuming $T_\mathrm{l}$ fixed, a fit of (12) to experimental data yields an extraordinarily low el–ph mass enhancement factor on the order of $(4 \pm 1) \times 10^{-4}$ that can be used to estimate a room-temperature el–ph scattering time of 15 ps [33, 35]. TRPE experiments thereby provide a direct time-domain view of the extraordinary current-carrying capacity and long ballistic electron mean-free paths found in metallic or semiconducting SWNTs [31, 37].

## 4 Semiconducting Tubes

As discussed in the contributions by Spataru et al., Ando, Saito et al., and Lefebvre et al., the optical properties of semiconducting SWNTs are governed by excitons, with exciton binding energies being substantial fractions of the bandgap energies. Measurements on a range of structurally distinct nanotube species using two-photon excitation spectroscopy (see the contribution by Lefebvre et al.) further showed that both the exciton binding energy and the corresponding bandgap energy scale inversely with the tube diameter [38]. A detailed understanding of the photophysics including spectral properties, exciton dynamics and their potential correlation with the geometrical structure of SWNTs are of interest from both a fundamental perspective and novel applications, in particular, in optoelectronics [39] (see also the contribution by Avouris et al.). For instance, the diameter-tunable PL emission from semiconducting SWNTs is particularly attractive for developing nanometer-sized near-infrared light emitters, and the realization would be greatly facilitated if the quantum efficiencies could be significantly enhanced. A detailed study

of various competing relaxation pathways with ultrafast spectroscopy should enable the elucidation of the physical reason for the extremely low quantum efficiency (see the contribution by Lefebvre et al.). Similarly, the application of ultrafast spectroscopy will also allow the quantification of the response time of semiconducting nanotube-based photodetectors and solar cells [39].

### 4.1 Exciton Dynamics

The dynamics of excitons is governed by their interactions with phonons, surface defects and impurities, charged carriers, as well as other excitons [12]. These interactions cause a variety of generally competing dynamical processes including intra- and intersubband relaxation, exciton dephasing and migration, trapping at defect and impurity states, as well as nonlinear exciton–exciton annihilation. A detailed study of exciton dynamics will thus provide fundamental insights into the microscopic aspects of these interactions and their influences on macroscopic properties, such as spectral lineshape, relaxation timescale and PL quantum yield, etc.

Resonant excitation of a semiconducting nanotube with femtosecond optical pulses creates a delocalized exciton whose length scale is determined by the extent of the wavefunction spread over the system under consideration. Ideally, the coherence size of the exciton is determined by the wavelength of the excitation field, but a reduction of the size is found in practice due to the scattering by phonons. Direct excitation of a higher-lying excitonic state of semiconducting SWNTs such as $E_{22}^S$ with pulses that are either in electronic resonance or non-resonance will undergo rapid intersubband relaxation to the energetically lowest excitonic state, the $E_{11}^S$ state, as a result of exciton–phonon interaction [5, 40, 41]. As recent calculations showed that each of the exciton states, such as $E_{11}^S$, $E_{22}^S$ and so on, corresponds to an exciton manifold [42], this will further lead to intrasubband relaxation.

Exciton recombination, one of the possible interband relaxation processes, can be either radiative or nonradiative. If one denotes the corresponding rate constants as $k_{\mathrm{r}}$ and $k_{\mathrm{nr}}$, respectively, the PL quantum yield can be written as $\Phi = k_{\mathrm{r}}/(k_{\mathrm{r}} + k_{\mathrm{nr}})$. Given the typical $\Phi$ value of $10^{-3}$–$10^{-4}$ found for semiconducting SWNTs dispersed individually with different surfactants at room temperature [15, 40, 43], it is immediately clear that the exciton dynamics probed by ultrafast optical spectroscopy must be dominated by nonradiative relaxation processes. This inference is fully consistent with the long radiative lifetime, with a timescale of the order of tens of nanoseconds [15, 44–46]. While it remains to be explored what kind of processes are involved in the nonradiative relaxation and whether they are intrinsic or extrinsic, the observation of a significantly increased PL yield from free-standing, individual nanotubes suggests that some extrinsic factors may play a substantial role [47] (see also the contribution by Lefebvre et al.).

When the intensity of the excitation pulse reaches a level such that the probability of creating two or more excitons per nanotube is no longer neg-

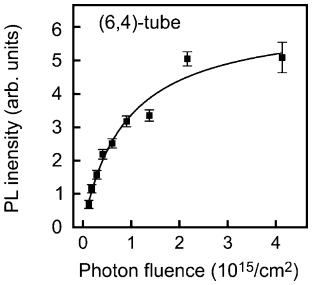


**Fig. 3.** Power dependence of the photoluminescence from a single confocally imaged (6,4) tube. The tube is excited off-resonantly at 800 nm and emission is detected in the 1110-nm range (from [17])

ligible, the interaction between excitons comes into play. This interaction is usually termed exciton–exciton annihilation in the language of molecular systems, and opens up an additional nonradiative decay channel. As a result, an accelerated kinetic decay and a decreased $\Phi$ value will be observed. The study of this nonlinear phenomenon provides information on the exciton motion in this one-dimensional (1D) system [48–53].

The discussion in the following will be divided into two subsections according to the excitation intensities employed in the experiments. The excitation density, i.e., the number of initial electron–hole (el–h) pair excitations per tube length, can be estimated, for example, using experimental or calculated photoabsorption cross sections of polyaromatic hydrocarbons [54, 55] as well as some recent experimental data from ropey and polydisperse SWNTs [54]. Due to the enhancement of exciton oscillator strengths in 1D systems both data sets probably underestimate the resonant photoabsorption cross sections $\sigma$ and suggest that $\sigma$ is in the $10^{-18}\,\mathrm{cm}^2\,\mathrm{atom}^{-1}$ range. For SWNTs with about 1 nm diameter, this implies an on-resonance photoabsorption cross section per nm of tube length well in excess of $10^{-16}\,\mathrm{cm}^2$. Experimentally, one finds that the power dependence of the PL signal from an individual (6,4) tube saturates around $5 \times 10^{15}$ photons $\mathrm{cm}^{-2}$ if excited off-resonantly at 800 nm (see Fig. 3) [17]. This intensity corresponds to the excitation of 100 to 500 excitons per micrometer of tube length. In the following, low excitation densities are thus defined as the fluence range below $2 \times 10^{14}$ photons $\mathrm{cm}^{-2}$ where the magnitude of optical transients as well as PL intensities scale linearly and the dynamics do not depend on excitation power.

### 4.2 Low Excitation Densities

As mentioned above, exciton dynamics in S-SWNTs depend on the excitation density, i.e., on the number of excitons generated on the tube per unit length [50, 53]. However, even low excitation densities – as identified by the linear dependence of transients and PL intensities on laser power – often correspond to the promotion of several excitons per tube. In fact, pump fluences at which only one exciton is excited per tube are experimentally difficult to realize simply because of the large number of atoms within a single tube

and due to the resulting large photoabsorption cross sections. Hence, our following discussion will be focused on the results obtained under the lowest excitation possible, in particular, on the data collected using streak cameras and TCSPC techniques. The high sensitivity of these techniques permits measurements at substantially lower excitation intensities than generally needed for other time-resolved experiments.

### 4.2.1 Intersubband Relaxation

Availability of tunable pulses with durations of $< 50$ fs allows one to resolve directly the intersubband exciton relaxation processes such as from the $E_{22}^S$ to the $E_{11}^S$ states. *Manzoni* et al. [56] reported so far the only study based on two-color pump-probe measurements on the SWNTs embedded in a polymethylmethacrylate matrix. The authors employed sub-10 fs visible pulses to excite the $E_{22}^S$ states of S-SWNTs resonantly, and the subsequent relaxation was probed at the corresponding $E_{11}^S$ states at 0.92 eV. The detected kinetics of induced transmission initiates with an instantaneous rise owing to the ground-state photobleaching, followed by a slower rise with a timescale of 40 fs corresponding to the relaxation from the $E_{22}^S$ to $E_{11}^S$ states. Similarly, a time constant of 65 fs was determined for the relaxation from the $E_{33}^S$ to the $E_{11}^S$ states.

As currently available samples are mostly polydisperse, usually with overlapping absorption spectra for at least some of the tube species, separate determination of the intersubband relaxation times for structurally distinct S-SWNTs remains to be explored. Future ensemble studies require either time-resolved PL measurements with an exceptionally high sensitivity and a time resolution better than sub-50 fs, or, perhaps more straightforwardly, transient absorption experiments with tunable sub-10 fs pulses provided that samples containing single tube types are available. The information gained from these studies will further enable verification of the predicted dependence of the intersubband relaxation times on nanotube chiralities [41].

### 4.2.2 Radiative Lifetime

Experimental determination of the radiative lifetime of S-SWNTs was first reported by *Hagen* et al. [46] and *Wang* et al. [15] based on time-resolved PL measurements on aqueous suspensions of SWNTs wrapped with surfactants. The experiments were performed by exciting the samples with $\sim 100$ fs pulses around 800 nm and by detecting the PL emission from various tube types with either a streak camera or by means of Kerr gating. These studies showed that the initial PL decay occurs on the 10-ps timescale with some variations from one study to the next. Given the low measured PL quantum yields of $10^{-3}$ or less [15, 40, 46, 57], it was concluded that nonradiative relaxation dominates the decay of the lowest optically active exciton. The radiative

lifetime was further estimated to be on the order of 10 and 110 ns, respectively. Even longer lifetimes of 260 ns [43] and 3.2 μs [58] were reported later by other groups based on time-resolved PL and transient absorption measurements. In comparison, theoretical calculations of *Spataru* et al. [44] and *Perebeinos* et al. [45] predicted, at room temperature, a radiative lifetime of the order of $\sim 10$ ns or $\sim 50$ ns, depending on whether only singlet excitonic states or both singlet and triplet states are assumed in the thermalization (see also the contributions by Spataru et al. and Avouris et al.).

It should be pointed out that a significantly increased PL yield up to $\sim 0.07$ was reported recently based on measurements on free-standing, individual tubes [47] (see also the contribution by Lefebvre et al.). Whether or not this will remarkably alter the radiative lifetime still needs to be tested by determining the PL lifetime.

### 4.2.3 Correlation of the PL Decay Timescales with the Tube Diameter

Selective detection of structurally distinct S-SWNTs, one at a time, with time-resolved PL spectroscopy at low excitation densities have allowed one to establish correlation of the PL decay time with the nanotube diameter ($d_t$). *Hertel* et al. [59] first reported a weak correlation based on the measurements on 6 small-diameter SWNTs and DWNT cores. In this experiment, several tube types were excited non-resonantly with sub-100 fs pulses at 795 nm and the emission from each tube type was spectrally selected and detected with a streak camera. The authors found that the decay time varies from $\sim 10$ ps for the tubes with $d_t = 0.76$ nm to 30 ps for those with $d_t = 0.88$ nm. Very recently, *Jones* et al. [60] reported a detailed time-resolved PL study of 15 different S-SWNT types with $d_t$ ranging from 0.76 to 1.04 nm. In this experiment, each desired tube type was separately measured using TCSPC by exciting resonantly its $E_{22}^S$ excitonic state and detecting the emission from the corresponding $E_{11}^S$ state. The electronic resonance in both the excitation and detection permits the exclusive probing of the tube type of interest. The authors found that in a 10-ns detection window, the PL decays can be accurately fitted to a biexponential function with two characteristic time constants. The dominant decay component $\tau_1$ increases from 60 to 200 ps with increasing $d_t$, while the lesser component $\tau_2$ increases from 200 ps to 4.8 ns. As shown in Fig. 4, strong linear correlations with $d_t$ are clearly evident for both time constants. The authors further proposed an extrinsic and an intrinsic model to explain the observed biexponential decay behavior.

One of the major discrepancies among the results reported so far is the dramatic differences in the time constant determined by different groups, even for the same type of tube coated with the same surfactant. For instance, the lifetime obtained for the (7,5) tube using SDS-solubilized samples varies from below 10 ps [59] to 29 ps [61] and further to 140 ps [43]. Another discrepancy is

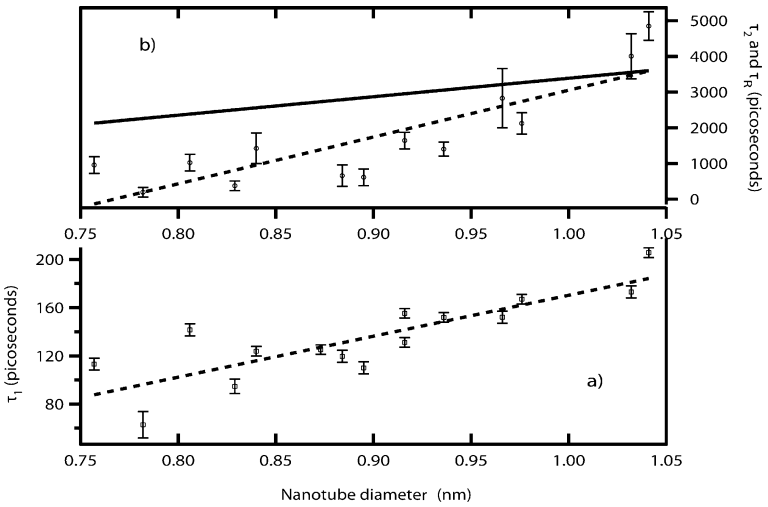


**Fig. 4.** Plot of decay times for (**a**) $\tau_1$ and (**b**) $\tau_2$ against nanotube diameter $d_t$ for 15 SWNT species, with *dotted lines* provided as a guide to the eye. The *solid line* in (**b**) corresponds to the theoretical prediction of the natural radiative lifetime, $\tau_R$ vs. $d_t$, for these SWNTs according to [45] (from [60])

the functional form needed to adequately describe the PL decay, either mono- [61], bi- [43, 60] or nonexponential [62], which further connects to a general lack of understanding of the underlying relaxation processes and relevant physical mechanisms. The discrepancies may arise from differences in time resolution, detection window, excitation intensity and sample preparation. Future experimental studies with better time resolution and sensitivity are highly desirable. Systematic measurements of PL decays at low temperatures and using samples dispersed with different surfactants are likely to be crucial for understanding the physical mechanism underlying the linear correlation of the PL decay times with $d_t$.

### 4.2.4 Environmental and Temperature Effects on Exciton Population Dynamics

As objects with large surface area, SWNTs are expected to be highly sensitive to their environment, which may strongly affect their electronic properties and excited-state dynamics. Ensemble and single-tube time-resolved studies at low excitation densities have enabled study of environmental effects on the dynamics underlying radiative and nonradiative decay from S-SWNTs. *Hertel* et al. [59] found that the PL decay time is highly sensitive to the surfactants used to suspend the nanotubes. Figure 5 shows the dependence of the PL decay of a (7,5) tube in different environments as measured using a streak camera. Here, the PL lifetime is found to increase from below 10 ps (i.e.,

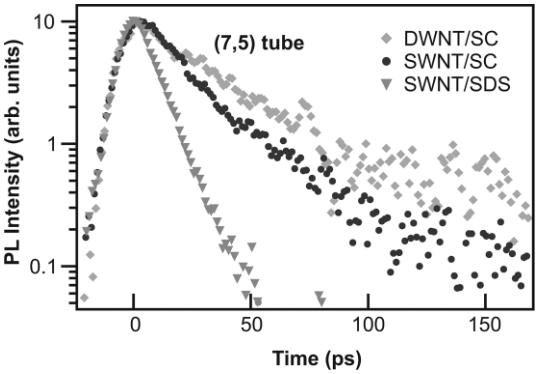


**Fig. 5.** $E_{11}^{S}$ photoluminescence decay in a (7,5) tube at room temperature for SWNTs in different environments. The longest lifetimes are here found for core tubes of the semiconducting (7,5) tube within double-wall carbon nanotubes (DWNTs) suspended by sodium cholate (SC), while the shortest lifetimes are observed in sodium-dodecyl sulfate (SDS)-suspended SWNTs (from [59])

the instrument response function) to 17 ps when the tube is suspended in SDS, sodium cholate, and 22 ps if it is the core of another larger tube in a DWNT. Such a sensitivity of the dynamics to the tube environments was also reported by *Ostojic* et al. [63] in an earlier pump-probe study. The authors found that the dynamics is strongly dependent on the pH of the aqueous solution of the SWNTs suspension. The detailed mechanisms that cause these effects still await future work, and possibilities may include variation of the exciton mobility and binding energy induced by environmental changes.

The aforementioned sensitivity of the dynamics to environmental factors observed from ensemble measurements was also found in single-tube TCSPC studies at cryogenic temperatures. *Hagen* et al. [17] found that there are considerable heterogeneities of the PL decay time that was found to vary by almost one order of magnitude from 20 ps to about 200 ps at 87 K (see Fig. 6). The heterogeneities in this study were attributed to the sensitivity to environmental effects or on-tube defects. Specifically, local variations of the dielectric environment, arising from inhomogeneities in the surfactant coating, for example, may be linked to changes in the alignment of exciton states. In the same study the authors also reported on the temperature dependence of single-tube PL lifetimes, which increase with decreasing temperature until a constant value is reached at around 60 K. In line with the large variation of the PL decay time found in the single-tube experiment, the kinetics obtained from recent ensemble measurements using time-resolved PL [62] and pump-probe measurements [64] at different temperatures exhibit more complex decay behavior. For instance, *Berger* et al. [62] found that the PL decay measured for the (9,4) tube type contains an initial fast component, which is temperature independent and is attributed to the presence of small residual

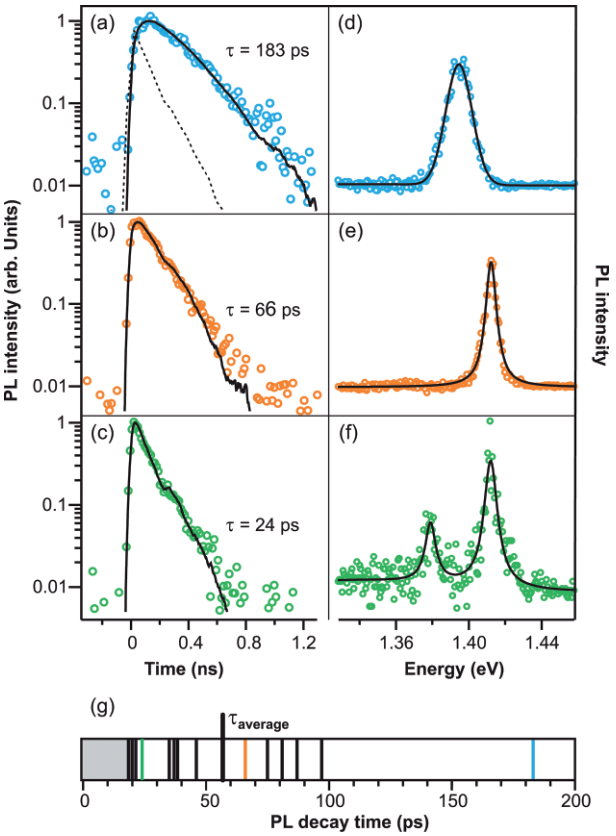


**Fig. 6.** Photoluminescence transients (**a**–**c**) and corresponding spectra (**d**–**f**) of three different single (6,4) SWNTs observed for excitation at 800 nm. Excited-state lifetimes at a sample temperature of 87 K for (**a**) and (**b**) and 67 K for (**c**) vary strongly from one tube to the next. (**g**) Bar graph of the distribution of all measured lifetimes at 87 K. The *gray area* on the *left* is the region not accessible due to the limited time resolution of the instrument (from [17])

bundles, and a slow component that is strongly dependent on temperature and is dominated by nonradiative processes down to 40 K. The observations from the ensemble and single-tube studies can either be attributed to the temperature dependence of the nonradiative decay rate or – as proposed recently – to the different emission strengths and temperature-dependent population distributions between the bright and slightly lower-lying dark excitons [65].

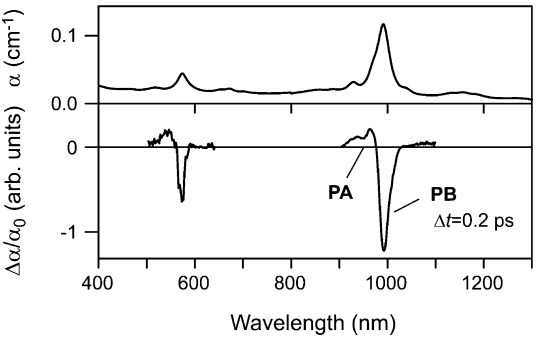


**Fig. 7.** Absorption spectrum (*upper panel*) and optical transient for $E_{22}^S$ excitation at 572 nm of an isopycnically (6,5)-enriched SWNT suspension (adapted from [66])

### 4.2.5 Transient Absorption of a Chirality-Enriched SWNT Preparation

Pump-probe spectroscopy provides a complementary means to explore the dynamics of optically excited states. Optical transients in the absorption spectra, however, are generally more difficult to assign to specific electronic processes if compared to PL studies, which in effect simply probe the excited-state population as given by $\rho_{\mathrm{ex}}$, the diagonal elements of the density matrix. If the dephasing times, however, are short with respect to the timescale of the energy and charge transfer or relaxation processes, we can use (11) for the analysis of transient spectra of optically active excitons in SWNT suspensions.

Figure 7 shows the absorption spectrum and transient spectrum of a chirality-enriched DNA-stabilized SWNT suspension in the visible and near-infrared regions [66]. The absorption spectrum is dominated by the optically active $E_{11}^S$ and $E_{22}^S$ states of the (6,5) tube at 993 nm and 572 nm, respectively. Analysis of absorption spectra suggests that roughly 35 % of the semiconducting tubes in this sample are of the (6,5) type. The high content of one specific species ensures that the dynamics observed in transient spectra are likewise dominated by the optical response of this particular species and to a much lesser extent by other tubes whose spectral features may overlap with the (6,5) tube. Resonant excitation of either the optically active $E_{11}^S$ or $E_{22}^S$ excitons, furthermore, allows mitigation of the influence of transients from other tubes by at least a factor of 5 due to resonantly increased absorption at the $E_{11}^S$ or $E_{22}^S$ energies [66].

The wavelength dependence of $\Delta\alpha(\omega)$ is shown in Fig. 8, from which it becomes evident that the spectral overlap of distinct photobleach (PB) and photoabsorption (PA) transients can be used to account for the seemingly complex wavelength dependence of optical transients. The same decomposition of the transient spectra into two similarly intense PB and PA components suggests that the PA component is due to a slightly blue-shifted (7.5 meV)

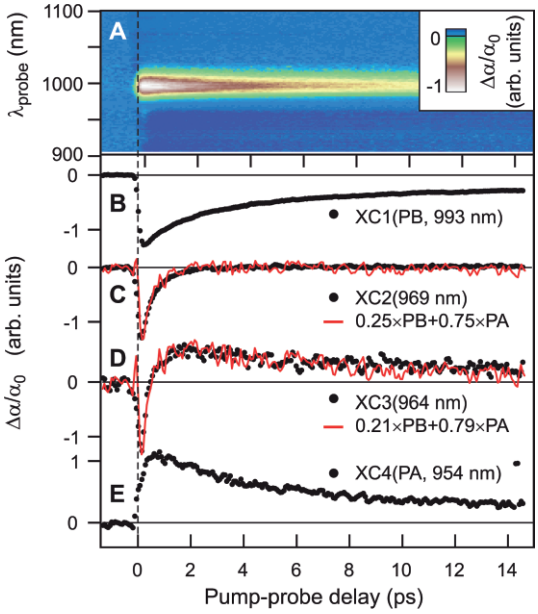


**Fig. 8.** (**A**) Optical transients as a function of probe wavelength and pump-probe delay for a DNA-stabilized (6,5)-enriched SWNT suspension. (**B**) Photobleach and (**E**) photoabsorption crosscorrelation traces at 993 nm and at 954 nm, respectively. The appropriately weighted sum of these two traces is shown to be able to account for the complex wavelength dependence of optical transients in (**C**) and (**D**). This illustrates that PB and PA represent two distinct but spectrally overlapping processes (adapted from [66])

transition [66]. The nature of this transition is currently still subject to debate [67, 68].

The nonexponential optical transients at longer pump-probe time delays (see Fig. 8) are found to exhibit power-law scaling in time with $\Delta\alpha(\omega) \approx t^{\gamma}$, where $\gamma$ is found to be $-0.45 \pm 0.03$ [66]. The power-law scaling can be interpreted as being due to some diffusion-limited relaxation process such as trapping in a disordered system [66] that is possibly associated with some type of exciton trapping mechanism. Pump-probe spectra from metallic carbon nanotubes, on the other hand, do not exhibit the power-law scaling type decay and return to the ground state significantly faster than their semiconducting counterparts [69].

### 4.3 High Excitation Densities

#### 4.3.1 Spectroscopic and Dynamic Signatures of High-Intensity Excitation

When the intensity of an excitation pulse reaches a level where the probability of creating two or more excitons per nanotube is no longer negligible, one has to consider the effects induced by this high excitation intensity. In such an intensity regime, the interaction between two excitons results in a nonlinear exciton–exciton annihilation process, which involves rapid relaxation of one exciton by releasing its energy to the second exciton, and consequently promoting the latter to a higher-energy excited state [70, 71]. The occurrence of this nonlinear process opens up an additional relaxation channel, which in turn strongly affects the exciton population dynamics detected using femtosecond fluorescence upconversion and pump-probe techniques.

Exciton–exciton annihilation in semiconducting nanotubes was first reported by *Fleming* and coworkers [50]. By employing a femtosecond fluorescence upconversion technique and an aqueous solution of micelle-dispersed HiPco nanotubes, the authors succeeded in measuring time-resolved fluorescence kinetics with sub-100 fs resolution. The measurements were performed on five structurally distinct nanotube species, namely, (8,3), (6,5), (7,5), (7,6) and (9,5) nanotubes. As an example, Fig. 9a shows the fluorescence kinetics detected at 1244 nm upon excitation at 660 nm for five different excitation densities. This combination of the excitation and emission wavelength selects exclusively the (9,5) tube type. As is clearly evident from Fig. 9a, the fluorescence decays show a strong intensity dependence, with faster decays as the excitation intensity increases. At the highest excitation intensity, the majority of excited population disappears within the first 500 fs. In addition, a nonlinear dependence of the maximum amplitude of the fluorescence signal on the excitation intensity is observed (Fig. 9b). A plot of the maximum amplitude versus the square root of excitation intensity shows a clear linear dependence (see inset in Fig. 9b). A similar decay behavior was observed for all other selected tube species, i.e., (8,3), (6,5), (7,5) and (7,6) (data not shown), which emit at 950, 975, 1024 and 1119 nm, respectively.

The strong excitation intensity dependence of the fluorescence decay in conjunction with the nonlinear correlation between the maximum fluorescence amplitude and the excitation intensity are indicative of the occurrence of exciton–exciton annihilation processes. Quantitative analysis of the fluorescence decays obtained at different excitation intensities further confirms this consideration. *Ma* et al. [50] found that the fluorescence decays can be satisfactorily described by the solution of a simple rate equation:

$$\frac{\mathrm{d}n_{\mathrm{ex}}(t)}{\mathrm{d}t} = -\frac{1}{2}\gamma n_{\mathrm{ex}}^2(t)\,, \tag{15}$$

where $n_{\mathrm{ex}}(t)$ denotes the population of excitons, and $\gamma$ represents a time-independent rate constant.

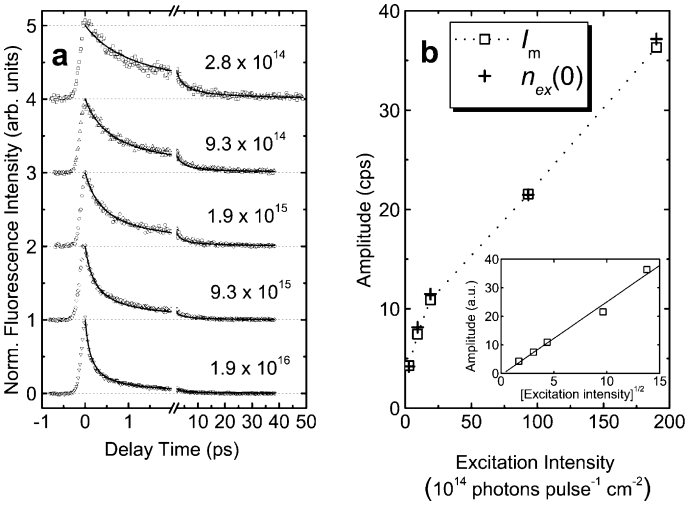


**Fig. 9.** (**a**) Normalized time-resolved fluorescence intensity vs. delay time for the (9,5) tube structure at different excitation intensities (in photons pulse$^{-1}$ cm$^{-2}$) detected at 1244 nm upon excitation at 660 nm. The *solid lines* represent global fits according to the solution of (15). (**b**) Plot of the maximum fluorescence intensity $I_{\rm m}$ and the fitted parameter $n_{\rm ex}(0)$ vs. the excitation intensities. The *dotted line* is drawn to guide the eye. The *inset* shows $I_{\rm m}$ plotted vs. the square root of the excitation intensity, and the *solid line* represents a linear fit to the data points. After [49]

The occurrence of exciton–exciton annihilation in semiconducting nanotubes was subsequently observed by *Wang* et al. [51]. In this study, the authors employed 150-fs laser pulses centered at a wavelength of 810 nm to excite an aqueous-solution sample of HiPco tubes dispersed individually with poly(acrylic acid). The fluorescence emission from various nanotube species was time resolved by an optical Kerr gating technique. Although the detection was not tube-type selective, the observed fluorescence kinetics shows a clear dependence on excitation intensity. Under high excitation intensity, a fast decay component emerges and its amplitude increases linearly with intensity. The annihilation rate, or the coefficient for the Auger recombination of two el–h pairs as termed by these authors, was estimated to be 0.8 ps$^{-1}$.

A similar intensity dependence of the kinetics was also observed using femtosecond pump-probe spectroscopy at wavelengths corresponding to the $E_{11}^S$ transitions of selective nanotube species [50, 51]. Evidently, frequency-resolved transient absorption spectroscopy appears particularly useful for elucidating the exciton–exciton annihilation phenomenon, and its application has led to identification of unique spectroscopic and dynamic signatures. As demonstrated by *Ma* et al. [48], electronically resonant excitation of the $E_{11}^S$ state of the (8,3) tube at 953 nm induces an instantaneous spectral re-

sponse at 660 nm, the location of the corresponding $E_{22}^S$ transition. The assignment of this response to the $E_{22}^S$ transition was confirmed by the similarity between the kinetics probed at 660 nm for excitation of the $E_{11}^S$ state and by direct $E_{22}^S$ excitation. On the other hand, the dependence of the amplitude of the transient absorption signal on the intensity of pump pulses at 953 nm differs for the kinetics probed at 660 and 953 nm. The former exhibits a linear dependence on pump fluence, whereas a saturating behavior is seen for the data obtained with a 953-nm probe pulse (Fig. 10a). Furthermore, the kinetics probed at 660 and 953 nm upon resonant excitation of the $E_{11}^S$ transition (Fig. 10b) are strongly correlated with each other. This correlation is manifested by an excellent match between the squared profile of the kinetics recorded at 953 nm and the kinetics measured at 660 nm (Fig. 10c).

The pump-intensity dependence of transient absorption spectra and of kinetics have been also observed by others [68, 72–74]. *Chou* et al. [72] reported two-color pump-probe experiments on an aqueous-solution sample of DNA-wrapped nanotubes synthesized by the CoMoCAT process, which is abundant in the (6,5) tube type. Upon excitation at 791 nm where an abundance of a large density of D-band phonons were excited, the kinetics probed at 990 nm, which is resonant with the $E_{11}^S$ state of the (6,5) tube type, can be satisfactorily described by a model function consisting of three exponential components. The corresponding timescales were determined to be $\sim 0.7$, 2–3 and 50 ps for the fast, intermediate and slow decay components, respectively, and the intermediate decay component was identified with the decay of these phonons. The authors further found that the timescales associated with the intermediate and slow decay components decrease substantially with increasing pump intensity. Two-color pump-probe measurements were also performed by *Huang* and *Krauss* [73] on a $D_2O$ solution of sodium dodecylbenzene sulfonate (SDBS) micelle-dispersed HiPco nanotubes under different pump fluences ranging from $2 \times 10^{13}$ to $5 \times 10^{15}$ photons/pulse cm$^2$. Following a procedure described in [75], the authors extracted time constants of 3.2 and 1.9 ps for the two and three el–h pairs states, respectively (see Fig. 11). Very recently, *Russo* et al. [74] reported a two-color pump-probe study on an aqueous solution of SDBS micelle-dispersed HiPco nanotubes at quite high excitation fluences corresponding to hundreds of excitons per micrometer length of a tube. Analysis of the kinetics obtained for the (8,6) and (7,6) tube types showed a power-law $1/\sqrt{\Delta t}$ dependence, where $\Delta t$ denotes the time delay between the pump and probe pulses. The authors ascribed this behavior to an exciton population relaxation via 1D diffusion-limited two-body recombination. However, such a time dependence was not observed in any previous studies, and the reason for the clear discrepancy between this result and others is currently unknown.

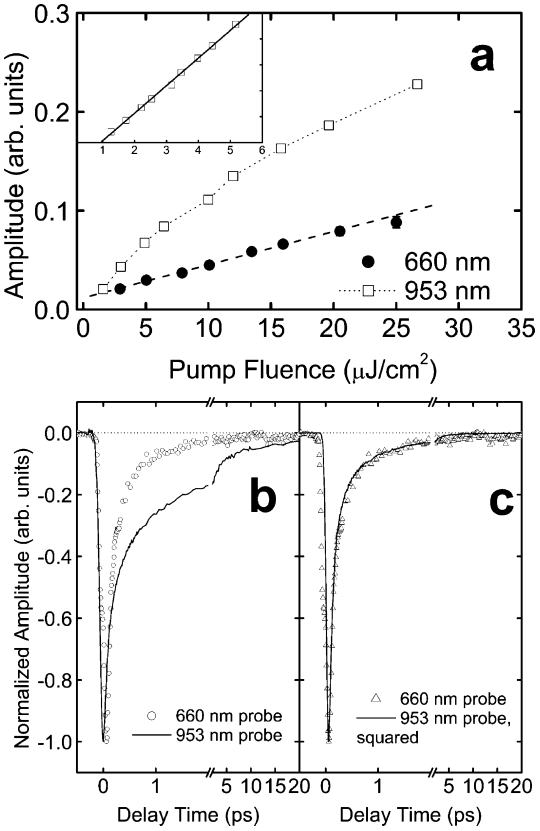


**Fig. 10.** (**a**) Plot of the maximum amplitude of the transient absorption kinetics probed at 660 nm (*filled circles*) and 953 nm (*open squares*) versus the intensity of the pump pulses at 953 nm. The *dashed line* is the linear fit of the data obtained with a 660-nm probe, and the *dotted line* is drawn to guide the eye for the data obtained with a 953-nm probe. The *inset* shows the 953-nm data, plotted vs. the scale of the square root of the pump intensity. The *solid line* represents the linear fit. (**b**) Kinetics probed at 660 (*open circles*) and 953 nm upon resonant excitation of the $E_{11}^S$ transition of the (8,3) tube at 953 nm. (**c**) Comparison of the squared profile at 953 nm (*solid line*) and the kinetics at 660 nm, both data being recorded with the 953-nm excitation. All kinetics shown in (**b**) and (**c**) are normalized at the signal maxima, after [49]

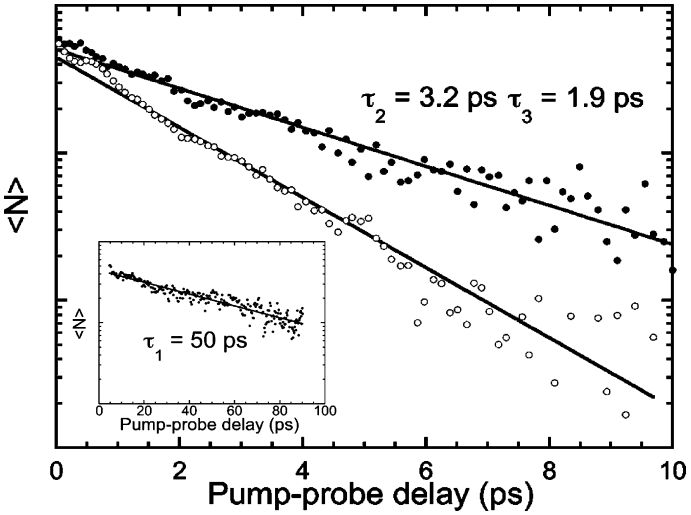


**Fig. 11.** The 1 el–h pair state dynamics (*inset*) and 2 (*solid circles*) and 3 (*open circles*) el–h pair dynamics extracted from transient absorption data probed at 1323 nm and fitted to a single exponential decay (*solid line*) (after [73])

### 4.3.2 Theoretical Advances

The need for describing and understanding the dynamics under high excitation intensities further stimulated theoretical interests. *Wang* et al. [51] first introduced a stochastic model of carrier dynamics for analyzing their experimental data obtained by time-resolved fluorescence measurements under different excitation intensities. The model explicitly includes Auger interactions and discrete occupancy of nanotubes by carriers, and numerical calculations showed good quantitative agreement with the experimental data. An analytical solution of this model was obtained later by *Barzykin* and *Tachiya* [52]. Very recently, *Wang* et al. [53], by attributing the process of the nonlinear exciton relaxation to exciton–exciton scattering, further derived an approximate expression for the Auger recombination (exciton annihilation) rate in terms of the exciton binding energy, optical matrix element and reduced carrier mass.

One major problem concerning the applicability of (15) to 1D systems was solved by *Valkunas* et al. [49] by considering explicitly the origin of the relaxation channels and exciton motion. This problem arises from the fact that (15) or its generalized form, with one or more linear terms in the right-hand side, is applicable to exciton–exciton annihilation in an extended system whose size is comparable with or larger than the exciton diffusion radius [70, 71]. For such systems, it is generally assumed that exciton–exciton annihilation is diffusion limited, and the corresponding annihilation rate depends on the dimensionality of the system. Use of a time-independent annihilation rate is

appropriate only for a system with a dimensionality ($d$) that is equal to or greater than 2. For systems with reduced dimension such as a SWNT, the annihilation rate limited by exciton diffusion becomes time dependent, given by $\gamma = \gamma_0/t^{1-(d/2)}$. However, it has been shown that an equation based on such an annihilation rate does not provide an appropriate description of the kinetics measured using fluorescence upconversion and transient absorption methods (with the exception of recent work by *Russo* et al. [74]). Thus, 1D diffusion as a limiting step for exciton–exciton annihilation does not provide the basis for a theoretical description of this process. *Valkunas* et al. [49] solved this problem by assuming that the nonlinear annihilation process predominantly proceeds between the coherent excitons within the SWNTs. Within this concept the results of *Russo* et al. may be considered as an indication of exciton–exciton annihilation defined by exciton migration from remote regions of the tube.

### 4.3.3 Exciton Dissociation

The annihilation of two $E_{11}^S$ excitons and the subsequent rapid relaxation from the high-lying excited state back to the $E_{11}^S$ state creates an exciton with a large excess energy. If this excess energy is greater than the exciton binding energy, exciton dissociation may occur. Such a dissociation was indeed identified previously in conjugated polymers [76]. Using the femtosecond transient absorption technique, *Ma* et al. [77] demonstrated the occurrence of exciton dissociation in semiconducting SWNTs. Employing pump pulses centered at 660 and 953 nm, the authors observed a new bleaching band in the transient absorption spectra, which peaks at 730 nm. This band cannot be assigned to the exciton transitions of the (8,3) tube type that was intentionally selected by the wavelength of the pump pulses, nor to those species that were unintentionally excited. Most importantly, the dependence of the kinetics detected at 730 nm on the intensity of 953-nm pump pulses indicates the occurrence of nonlinear relaxation, and a satisfactory description of the 730-nm kinetics probed under the highest pump intensity was obtained with a model involving Auger recombination of charge carriers. This strongly suggests that the 730-nm band does not originate from an exciton but instead from an el–h continuum [75, 78, 79]. Knowing the nature of this new band, it is straightforward to calculate an exciton binding energy of 0.41 eV for the (8,3) nanotube. This value is very close to the experimental results obtained using two-photon fluorescence excitation spectroscopy [80, 81], and this determination does not require any assumption for the model for the el–h interaction.

Since observation of this phenomenon was reported so far only for the (8,3) tube type, further studies on different semiconducting SWNT species under similar experimental conditions are highly desirable. Use of chirality-enriched SWNT samples will be particularly helpful in avoiding ambiguity.

## 5 Comparison of S-SWNTs with π-Conjugated Polymers

The π-conjugated polymers are the first quasi-1D systems that have been studied extensively over the last 25 years. π-conjugated polymers possess quasi-1D electronic states and consequently also a 1D density of states. The lateral quantization may result in structured conduction and valence bands with subbands and van Hove singularities. The properties of such electronic systems are determined by the ratio of two characteristic energies, namely the electron–electron Coulomb interaction, ($E_{\mathrm{Coul}}$) and the confinement energy, $\Delta E$ of lateral quantization (energy separation, $\Delta E$ between the van Hove singularities). In many π-conjugated systems $E_{\mathrm{Coul}} > \Delta E$. Under these conditions it is not possible to consider electrons and holes as independent, noninteracting particles, as in semiconductor quantum dots or nanorods.

Unsubstituted π-conjugated polymers usually possess inversion symmetry, and thus their eigenstates are classified as having either even-parity $nA_{\mathrm{g}}$ or odd-parity $n'B_{\mathrm{u}}$, where both the $n$ and $n'$ are integers that denote the order within an exciton band. Two important singlet exciton levels ($1^1B_{\mathrm{u}}$ and $m^1A_{\mathrm{g}}$) and a double-excitation-type singlet level ($k^1A_{\mathrm{g}}$) are shown in Fig. 12 [82]; their electron configurations are also shown for clarity. The $m^1A_{\mathrm{g}}$ is a specific excited state above the $1^1B_{\mathrm{u}}$ level, whereas the $k^1A_{\mathrm{g}}$ excited state may be due to a biexciton state, i.e., a bound state of two $1^1B_{\mathrm{u}}$ excitons. The $m^1A_{\mathrm{g}}$ level is known to have strong dipole moment coupling to $1B_{\mathrm{u}}$, as deduced from the various optical nonlinear spectra of π-conjugated polymers analyzed in terms of the "four essential states" model [83]. It is therefore expected that two strong optical transitions form following the $1^1B_{\mathrm{u}}$ photogeneration: $\mathrm{PA}_1$ and $\mathrm{PA}_2$, as shown in Fig. 12a, where PA denotes photoinduced absorption. As the $m^1A_{\mathrm{g}}$ state is below the continuum band threshold state $n^1B_{\mathrm{u}}$, the energy of the $\mathrm{PA}_1$ band gives the lower limit of exciton binding energy. A similarly calculated electronic structure of an S-SWNT is shown in Fig. 12b, which exhibits multiple energy manifolds $n = 1, 2, \ldots$, etc. Within each $n$, there occur optically dark excitons D$n$ a few $k_{\mathrm{B}}T$ below the optically allowed exciton Ex$n$. The occurrence of these dark excitons represents one of the differences between S-SWNTs and π-conjugated polymers.

*Vardeny* and coworkers [84] found that the transient absorption spectra obtained using films of S-SWNTs and two π-conjugated semiconducting polymers, poly(dioctyloxy)para-phenylene vinylene (DOO-PPV) and poly(9,9-dioctylfluorene) (PFO), are quite similar. As an example, Fig. 13 shows the spectra collected at $\Delta t = 0$, and it is clear that all the spectra contain both negative PA and positive photobleaching (PB) or stimulated emission (SE) bands. In neither sample do the authors obtain a PA spectrum that increases at low energy in the shape of free-carrier absorption, viz., $\Delta\alpha \sim \omega^2$. Instead, the PA spectra are in the form of distinct photoinduced bands $\mathrm{PA}_1$ and $\mathrm{PA}_2$ associated with specific optical transitions of the primary photoexcitations in the samples, which are therefore not free carriers. The authors

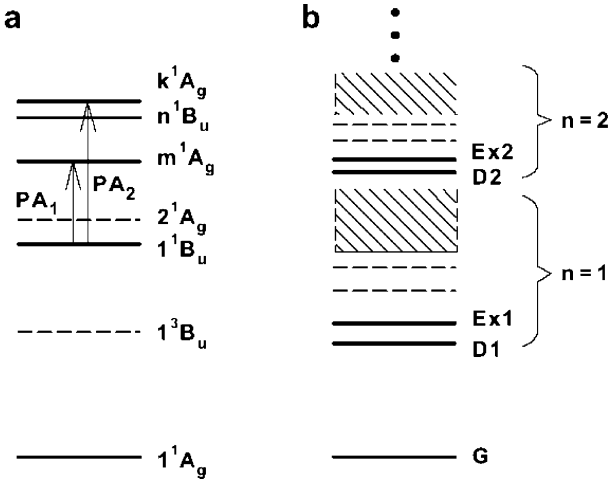


**Fig. 12.** Schematics of the excitonic electronic structures of (**a**) a light-emissive $\pi$-conjugated polymer and (**b**) an S-SWNT. In (**a**) the lowest triplet exciton $1^3B_u$ occurs below the lowest singlet exciton $1^1B_u$. The lowest two-photon state $2^1A_g$ is composed of two triplets and plays a weak role in nonlinear absorption. Transient PA (photoabsorption) is from the $1^1B_u$ to the $m^1A_g$ two-photon exciton that occurs below the continuum band threshold state $n^1B_u$, and to a high-energy $k^1A_g$ state that occurs deep inside the continuum band. In (**b**), Ex$n$ and D$n$ are dipole-allowed and dipole-forbidden excitons, respectively (after [84])

further found, through measurements of the kinetics at selected probe wavelengths, that the PA and their respective PB (or SE) bands in both polymers and S-SWNTs are correlated to each other. This correlation is manifested by very similar dynamics and therefore they should share a common origin, namely, the same primary excitation, which is the photogenerated exciton. A similar correlation was also observed by *Hertel* and coworkers [66] on a chirality-enriched DNA-stabilized SWNT suspension.

Based on the analysis of the similarities between the transient absorption spectra and kinetics measured on the films of S-SWNTs and $\pi$-conjugated polymers, *Vardeny* and coworkers [84] concluded that the origin of the low-energy $PA_1$ in S-SWNTs is the excited-state absorption from Ex1 and D1 to higher-energy two-photon excitons. The broad nature of the $PA_1$ band in the S-SWNTs arises from the inhomogeneity of the experimental sample, with SWNT bundles that contain a distribution of S-SWNTs with different diameters and exciton binding energies. The authors also speculated that the $n$ =1 continuum band lies between the peaks of the $PA_1$ and $PA_2$ bands. This analysis further enabled the authors to construct the vertical dashed line in Fig. 13c, which identifies the threshold of the continuum band for the S-SWNTs with the largest diameter in the film. Exciton binding energies of ca. 0.4 eV are then predicted for those S-SWNTs in the film that dominate

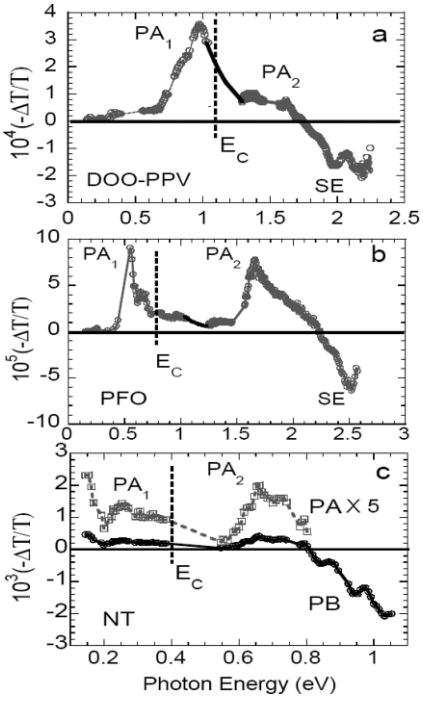


**Fig. 13.** Transient absorption spectra at $t = 0$ of films of DOO-PPV (**a**), PFO (**b**), and isolated SWNT in polyvinyl alcohol matrix (**c**). Various PA, PB, and SE bands are assigned. The *vertical dashed lines* at $E_C$ between $PA_1$ and $PA_2$ denote the estimated continuum band onset. In (**a**) and (**b**), the *vertical dashed lines* were drawn based on the information obtained from two-photon absorption and electroabsorption experiments [84]. The *corresponding line* in (**c**) was drawn by scaling the result shown in (**b**) according to the ratio of their $PA_1$ peak energies (after [84])

the nonlinear absorption, which is similar to the results of two-photon PL excitation [80, 81] and femtosecond transient absorption [77] spectroscopy. The successful transferability of the parameters from PPV to S-SWNTs then suggests that the Coulomb interaction parameters as well as the background dielectric constants in these two classes of materials are close in magnitude. This in turn justifies the use of $\pi$-electron models for the S-SWNTs, at least for the S-SWNTs with the largest diameter, which dominate the nonlinear absorption.

## 6 Summary

Even though this field of carbon-nanotube research has been in existence for only a few years, progress in studies of carrier and exciton dynamics with ultrafast spectroscopy has been both rapid and fascinating. Application of TRPE, time-resolved fluorescence and femtosecond transient absorption spectroscopy has enabled elucidation in real time of the el–ph interactions in metallic tubes, and exciton relaxation processes and the underlying physical mechanisms in semiconducting SWNTs. It is now clear that excitation of semiconducting SWNTs with intense ∼100 fs laser pulses leads to dynamics dominated by a remarkable exciton–exciton annihilation process. Studies

employing low excitation intensity allow the timescales of the intersubband and radiative relaxation processes to be determined, along with the intrinsic spectral and dynamical properties, and the profound extrinsic effects of tube environment and temperature.

On the other hand, there are still significant inconsistencies and/or discrepancies between the results and their interpretations reported by different laboratories, which require further experimental and theoretical studies. Besides implementation of more sophisticated spectroscopic techniques, we believe that it is crucial to have samples with well-characterized purities and distribution of tube lengths. This will enable more precise quantification of the level of excitation intensity used for experiments. Another, perhaps equally important, area to explore via controlled studies concerns the potential effects arising from defects and/or unintentional doping during synthesis or post-growth processing.

We envision the emergence of several new research directions in the near future. These will include direct assessment of exciton coherence and relevant dephasing timescales, elucidation of the role of phonon and dark excitonic states in the exciton relaxation processes, quantification of exciton dissociation and discrimination of intrinsic dynamical processes from those induced by external factors. These new studies will involve time-resolved mid-infrared, terahertz, two-photon and 2D electronic spectroscopies. Besides these ensemble studies, time-resolved single-tube spectroscopy with various time-resolution and detection sensitivities will be also increasingly exploited. It is likely that the level of research activity in this field will continue to increase.

**Acknowledgements**

The work at Berkeley was supported by the NSF. Y.-Z. Ma thanks M. W. Graham for help with LaTeX, Drs. G. Rumbles, Libai Huang and T. D. Krauss for providing eps files of Figs. 4 and 11. L. Valkunas acknowledges the Lithuanian Science and Studies Foundation. T. Hertel acknowledges support by the NSF under grants #DMR0606505 and #DGE0333392 and by the Petroleum Research Fund under grant #PRF 44479-AC10. Z. V. Vardeny wishes to acknowledge Drs. O. Korovyanko and C.-X. Sheng for the transient absorption measurements, Prof. Baughman for the SWNT samples, and Prof. S. Mazumdar for fruitful discussions.

## References

[1] C. Rullière (Ed.): *Femtosecond Laser Pulses: Principles and Experiments*, 2nd ed. (Springer, New York 2005) please provide place of printing for [1].

[2] J.-C. Diels, W. Rudolph: *Ultrashort Laser Pulse Phenomena* (Academic Press, San Diego, New York 1996)

[3] H. van Amerongen, R. van Grondelle: Transient absorption spectroscopy in study of processes and dynamics in biology, Method. Enzymol. **246**, 201–226 (1995)
[4] R. Jimenez, G. R. Fleming: Ultrafast spectroscopy of photosynthetic systems, in J. Amesz, A. J. Hoff (Eds.): *Biophysical Techniques in Photosynthesis* (Kluwer, Dordrecht 1996) pp. 63–73
[5] Y.-Z. Ma, L. Valkunas, S. L. Dexheimer, G. R. Fleming: Ultrafast exciton dynamics in semiconducting single-walled carbon nanotubes, Mol. Phys. **104**, 1179–1189 (2006)
[6] H. Petek, S. Ogawa: Femtosecond time-resolved two-photon photoemission studies of electron dynamics in metals, Prog. Surf. Sci. **56**, 239–310 (1998)
[7] T. Hertel, R. Fasel, G. Moos: Charge-carrier dynamics in single-walled carbon nanotube bundles: A time-domain study, Appl. Phys. A **75**, 449–465 (2002)
[8] M. Bauer: Femtosecond ultraviolet photoelectron spectroscopy of ultrafast surface processes, J. Phys. D Appl. Phys. **38**, R253–R267 (2005)
[9] M. Wolf: Femtosecond dynamics of electronic excitations at metal surfaces, Surf. Sci. **377**, 343–349 (1997)
[10] P. M. Echenique, R. Berndt, E. V. Chulkov, T. H. Fausterd, A. Goldmann, U. Höfer: Decay of electronic excitations at metal surfaces, Surf. Sci. Rep. **52**, 219–317 (2004)
[11] R. W. Schoenlein, W. Z. Lin, J. G. Fujimoto, G. L. Eesley: Femtosecond studies of nonequilibrium electronic processes in metals, Phys. Rev. Lett. **58**, 1680–1683 (1987)
[12] J. Shah: *Ultrafast Spectroscopy of Semiconductors and Semiconductor Nanostructures*, 2nd ed., Springer series in solid-state sciences (Springer, Berlin, Heidelberg 1999)
[13] M. A. Kahlow, W. Jarzeba, T. P. DuBruil, P. F. Barbara: Ultrafast emission spectroscopy in the ultraviolet by time-gated upconversion, Rev. Sci. Instrum. **59**, 1098–1109 (1988)
[14] J. Shah: Ultrafast luminescence spectroscopy using sum frequency generation, IEEE J. Quantum Electron. **24**, 276–288 (1988)
[15] F. Wang, G. Dukovic, L. E. Brus, T. F. Heinz: Time-resolved fluorescence of carbon nanotubes and its implication for radiative lifetimes, Phys. Rev. Lett. **92**, 177401 (2004)
[16] D. V. O'Connor, D. Phillips: *Time-Correlated Single Photon Counting* (Academic Press, London, Orlando 1984)
[17] A. Hagen, M. Steiner, M. B. Raschke, C. Lienau, T. Hertel, H. Qian, A. J. Meixner, A. Hartschuh: Exponential decay lifetimes of excitons in individual single-walled carbon nanotubes, Phys. Rev. Lett. **95**, 197401 (2005)
[18] G. R. Fleming: *Chemical Applications of Ultrafast Spectroscopy*, The International series of monographs on chemistry (Oxford University Press, New York 1985)
[19] J. D. Jackson: *Classical Electrodynamics*, 3rd ed. (Wiley, New York 1999)
[20] N. Bloembergen: *Nonlinear Optics* (Benjamin, New York 1965)
[21] M. Born, E. Wolf: *Principles of Optics*, 6th ed. (Pergamon, Oxford 1980)
[22] S. Mukamel: *Principles of Nonlinear Optical Spectroscopy* (Oxford University Press, New York 1995)
[23] K. Blum: *Density Matrix Theory and Applications* (Plenum, New York 1981)

[24] M. Cho, H. M. Vaswani, T. Brixner, J. Stenger, G. R. Fleming: Exciton analysis in 2D electronic spectroscopy, J. Phys. Chem. B **109**, 10542–10556 (2005)
[25] T. Joo, Y. Jia, J.-Y. Yu., M. J. Lang, G. R. Fleming: Third-order nonlinear time domain probes of solvation dynamics, J. Chem. Phys. **104**, 6089–6108 (1996)
[26] J. E. Fischer, H. Dai, A. Thess, R. Lee, N. M. Hanjani, D. L. Dehaas, R. E. Smalley: Metallic resistivity in crystalline ropes of single-wall carbon nanotubes, Phys. Rev. B **55**, R4921–R4924 (1997)
[27] J. Hone, I. Ellwood, M. Muno, A. Mizel, M. L. Cohen, A. Zettl, A. G. Rinzler, R. E. Smalley: Thermoelectric power of single-walled carbon nanotubes, Phys. Rev. Lett. **80**, 1042–1045 (1998)
[28] L. X. Benedict, V. H. Crespi, S. G. Louie, M. L. Cohen: Static conductivity and superconductivity of carbon nanotubes: Relations between tubes and sheets, Phys. Rev. B **52**, 14935–14940 (1995)
[29] J. W. Mintmire, B. I. Dunlap, C. T. White: Are fullerene tubules metallic?, Phys. Rev. Lett. **68**, 631–634 (1992)
[30] R. A. Jishi, M. S. Dresselhaus, G. Dresselhaus: Electron–phonon coupling and the electrical conductivity of fullerene nanotubules, Phys. Rev. B **48**, 11385–11389 (1993)
[31] S. Frank, P. Poncharal, Z. L. Wang, W. A. de Heer: Carbon nanotube quantum resistors, Science **280**, 1744–1746 (1998)
[32] P. Avouris, T. Hertel, R. Martel, T. Schmidt, H. R. Shea, R. E. Walkup: Carbon nanotubes: Nanomechanics, manipulation, and electronic devices, Appl. Surf. Sci. **141**, 201–209 (1999)
[33] T. Hertel, G. Moos: Electron–phonon interaction in single-wall carbon nanotubes: A time-domain study, Phys. Rev. Lett. **84**, 5002–5005 (2000)
[34] S. I. Anisimov, B. L. Kapeliov, T. L. Perel'man: Electron-emission from surface of metals induced by ultrashort laser pulses, Zh. Eksp. Teor. Fiz. **66**, 776–781 (1974)
[35] G. Moos, R. Fasel, T. Hertel: Temperature dependence of electron to lattice energy-transfer in single-wall carbon nanotube bundles, J. Nanosci. Nanotechnol. **3**, 145–149 (2003)
[36] P. B. Allen: Theory of thermal relaxation of electrons in metals, Phys. Rev. Lett. **59**, 1460–1463 (1987)
[37] T. Durkop, S. A. Getty, E. Cobas, M. S. Fuhrer: Extraordinary mobility in semiconducting carbon nanotubes, Nano Lett. **4**, 35–39 (2004)
[38] G. Dukovic, F. Wang, D. Song, M. Y. Sfeir, T. F. Heinz, L. E. Brus: Structural dependence of excitonic optical transitions and band-gap energies in carbon nanotubes, Nano Lett. **5**, 2314–2318 (2005)
[39] P. Avouris, J. Chen, M. Freitag, V. Perebeinos, J. C. Tsang: Carbon nanotube optoelectronics, Phys. Stat. Sol. B **243**, 3197–3203 (2006)
[40] M. J. O'Connell, S. M. Bachilo, C. B. Huffman, V. C. Moore, M. S. Strano, E. H. Haroz, K. L. Rialon, P. J. Boul, W. H. Noon, C. Kittrell, J. P. Ma, R. H. Hauge, R. B. Weisman, R. E. Smalley: Band gap fluorescence from individual single-walled carbon nanotubes, Science **297**, 593–596 (2002)
[41] Y. Oyama, R. Saito, K. Sato, J. Jiang, G. Samsonidze, A. Grüneis, Y. Miyauchi, S. Maruyama, A. Jorio, G. Dresselhaus, M. S. Dresselhaus: Photoluminescence intensity of single-wall carbon nanotubes, Carbon **44**, 873–879 (2006)

[42] Y.-Z. Ma, C. D. Spataru, L. Valkunas, S. G. Louie, G. R. Fleming: Spectroscopy of zigzag single-walled carbon nanotubes: Comparing femtosecond transient absorption spectra with ab initio calculations, Phys. Rev. B **74**, 085402 (2006)
[43] M. Jones, C. Engtrakul, W. K. Metzger, R. J. Ellingson, A. J. Nozik, M. J. Heben, G. Rumbles: Analysis of photoluminescence from solubilized single-walled carbon nanotubes, Phys. Rev. B **71**, 115426 (2005)
[44] C. D. Spataru, S. Ismail-Beigi, R. B. Capaz, S. G. Louie: Theory and ab initio calculation of radiative lifetime of excitons in semiconducting carbon nanotubes, Phys. Rev. Lett. **95**, 247402 (2005)
[45] V. Perebeinos, J. Tersoff, P. Avouris: Radiative lifetime of excitons in carbon nanotubes, Nano Lett. **5**, 2495–2499 (2005)
[46] A. Hagen, G. Moos, V. Talalaev, T. Hertel: Electronic structure and dynamics of optically excited single-walled carbon nanotubes, Appl. Phys. A **78**, 1137–1145 (2004)
[47] J. Lefebvre, D. G. Austing, J. Bond, P. Finnie: Photoluminescence imaging of suspended single-walled carbon nanotubes, Nano Lett. **6**, 1603–1608 (2006)
[48] Y.-Z. Ma, L. Valkunas, S. L. Dexheimer, S. M. Bachilo, G. R. Fleming: Femtosecond spectroscopy of optical excitations in single-walled carbon nanotubes: Evidence for exciton-exciton annihilation, Phys. Rev. Lett. **94**, 157402 (2005)
[49] L. Valkunas, Y.-Z. Ma, G. R. Fleming: Exciton-exciton annihilation in single-walled carbon nanotubes, Phys. Rev. B **73**, 115432 (2006)
[50] Y.-Z. Ma, J. Stenger, J. Zimmermann, S. M. Bachilo, R. E. Smalley, R. B. Weisman, G. R. Fleming: Ultrafast carrier dynamics in single-walled carbon nanotubes probed by femtosecond spectroscopy, J. Chem. Phys. **120**, 3368–3373 (2004)
[51] F. Wang, G. Dukovic, E. Knoesel, L. E. Brus, T. F. Heinz: Observation of rapid Auger recombination in optically excited semiconducting carbon nanotubes, Phys. Rev. B **70**, 241403 (2004)
[52] A. V. Barzykin, M. Tachiya: Stochastic models of carrier dynamics in single-walled carbon nanotubes, Phys. Rev. B **72**, 075425 (2005)
[53] F. Wang, Y. Wu, M. S. Hybertsen, T. F. Heinz: Auger recombination of excitons in one-dimensional systems, Phys. Rev. B **73**, 245424 (2006)
[54] M. F. Islam, D. E. Milkie, C. L. Kane, A. G. Yodh, J. M. Kikkawa: Direct measurement of the polarized optical absorption cross section of single-wall carbon nanotubes, Phys. Rev. Lett. **93**, 037404 (2004)
[55] G. Malloci, G. Mulas, C. Joblin: Electronic absorption spectra of PAHs up to vacuum UV – towards a detailed model of interstellar PAH photophysics, Astron. Astrophys. **426**, 105–117 (2004)
[56] C. Manzoni, A. Gambetta, E. Menna, M. Meneghetti, G. Lanzani, G. Cerullo: Intersubband exciton relaxation dynamics in single-walled carbon nanotubes, Phys. Rev. Lett. **94**, 207401 (2005)
[57] J. Crochet, M. Clemens, T. Hertel: Quantum yield heterogeneities of aqueous single-wall carbon nanotube suspensions, J. Am. Chem. Soc. **129**, 8058–8059 (2007)
[58] C.-X. Sheng, Z. V. Vardeny, A. B. Dalton, R. H. Baughman: Exciton dynamics in single-walled nanotubes: Transient photoinduced dichroism and polarized emission, Phys. Rev. B **71**, 125427 (2005)

[59] T. Hertel, A. Hagen, V. Talalaev, K. Arnold, F. Hennrich, M. Kappes, S. Rosenthal, J. McBride, H. Ulbricht, E. Flahaut: Spectroscopy of single- and double-wall carbon nanotubes in different environments, Nano Lett. **5**, 511–514 (2005)
[60] M. Jones, W. K. Metzger, T. J. McDonald, C. Engtrakul, R. J. Ellingson, G. Rumbles, M. J. Heben: Extrinsic and intrinsic effects on the excited-state kinetics of single-walled carbon nanotubes, Nano Lett. **7**, 300–306 (2007)
[61] S. Reich, M. Dworzak, A. Hoffmann, C. Thomsen, M. S. Strano: Excited-state carrier lifetime in single-walled carbon nanotubes, Phys. Rev. B **71**, 033402 (2005)
[62] S. Berger, C. Voisin, G. Cassabois, C. Delalande, P. Roussignol, X. Marie: Temperature dependence of exciton recombination in semiconducting single-wall carbon nanotubes, Nano Lett. **7**, 398–402 (2007)
[63] G. N. Ostojic, S. Zaric, J. Kono, M. S. Strano, V. C. Moore, R. H. Hauge, R. E. Smalley: Interband recombination dynamics in resonantly excited single-walled carbone nanotubes, Phys. Rev. Lett. **92**, 117402 (2004)
[64] Y.-Z. Ma, L. Valkunas, S. M. Bachilo, G. R. Fleming: Temperature effects on femtosecond transient absorption kinetics of semiconducting single-walled carbon nanotubes, Phys. Chem. Chem. Phys. **8**, 5689–5693 (2006)
[65] I. B. Mortimer, R. J. Nicholas: Role of bright and dark excitons in the temperature-dependent photoluminescence of carbon nanotubes, Phys. Rev. Lett. **98**, 027404 (2007)
[66] Z. P. Zhu, J. Crochet, M. S. Arnold, M. C. Hersam, H. Ulbricht, D. Resasco, T. Hertel: Pump-probe spectroscopy of exciton dynamics in (6,5) carbon nanotubes, J. Phys. Chem. C **111**, 3831–3835 (2007)
[67] G. N. Ostojic, S. Zaric, J. Kono, V. C. Moore, R. H. Hauge, R. E. Smalley: Stability of high-density one-dimensional excitons in carbon nanotubes under high laser excitation, Phys. Rev. Lett. **94**, 097401 (2005)
[68] O. J. Korovyanko, C.-X. Sheng, Z. V. Vardeny, A. B. Dalton, R. H. Baughman: Ultrafast spectroscopy of excitons in single-walled carbon nanotubes, Phys. Rev. Lett. **92**, 017403 (2004)
[69] Z. Zhu, M. S. Arnold, M. C. Hersam, T. Hertel: unpublished
[70] L. Valkunas, G. Trinkunas, V. Liuolia: Exciton annihilation in molecular aggregates, in D. L. Andrews, A. A. Demidov (Eds.): *Resonance Energy Transfer* (Wiley, Chichester 1999) pp. 244–307
[71] H. van Amerongen, L. Valkunas, R. van Grondelle: *Photosynthetic Excitons* (World Scientific, Singapore, New Jersey, London, Hongkong 2000)
[72] S. G. Chou, M. F. DeCamp, J. Jiang, G. G. Samsonidze, E. B. Barros, F. Plentz, A. Jorio, M. Zheng, G. B. Onoa, E. D. Semke, A. Tokmakoff, R. Saito, G. Dresselhaus, M. S. Dresselhaus: Phonon-assisted exciton relaxation dynamics for a (6,5)-enriched DNA-wrapped single-walled carbon nanotube sample, Phys. Rev. B **72**, 195415 (2005)
[73] L. Huang, T. D. Krauss: Quantized bimolecular Auger recombination of excitons in single-walled carbon nanotubes, Phys. Rev. Lett. **96**, 057407 (2006)
[74] R. M. Russo, E. J. Mele, C. L. Kane, I. V. Rubtsov, M. J. Therien, D. E. Luzzi: One-dimensional diffusion-limited relaxation of photoexcitations in suspensions of single-walled carbon nanotubes, Phys. Rev. B **74**, 041405(R) (2006)

[75] V. I. Klimov, A. A. Mikhailovsky, D. W. McBranch, C. A. Leatherdale, M. G. Bawendi: Quantization of multiparticle Auger rates in semiconductor quantum dots, Science **287**, 1011–1013 (2000)
[76] M. A. Stevens, C. Silva, D. M. Russell, R. H. Friend: Exciton dissociation mechanisms in the polymeric semiconductors poly(9,9-dioctylfluorene) and poly(9,9-dioctylfluorene-co-benzothiadiazole), Phys. Rev. B **63**, 165213 (2001)
[77] Y.-Z. Ma, L. Valkunas, S. M. Bachilo, G. R. Fleming: Exciton binding energy in semiconducting single-walled carbon nanotubes, J. Phys. Chem. B **109**, 15671–15674 (2005)
[78] M. Ghanassi, M. C. Schanne-Klein, F. Hache, A. I. Ekimov, D. Ricard, C. Flytzanis: Time-resolved measurements of carrier recombination in experimental semiconductor-doped glasses: Confirmation of the role of Auger recombination, Appl. Phys. Lett. **62**, 78–80 (1993)
[79] H. Htoon, J. A. Hollingsworth, R. Dickerson, V. I. Klimov: Effect of zero- to one-dimensional transformation on multiparticle Auger recombination in semiconductor quantum rods, Phys. Rev. Lett. **91**, 227401 (2003)
[80] F. Wang, G. Dukovic, L. E. Brus, T. F. Heinz: The optical resonances in carbon nanotubes arise from excitons, Science **308**, 838–841 (2005)
[81] J. Maultzsch, R. Pomraenke, S. Reich, E. Chang, D. Prezzi, A. Ruini, E. Molinari, M. S. Strano, C. Thomsen, C. Lienau: Exciton binding energies in carbon nanotubes from two-photon photoluminescence, Phys. Rev. B **72**, 241402(R) (2005)
[82] S. N. Dixit, D. Guo, S. Mazumdar: Essential-states mechanism of optical nonlinearity in $\pi$-conjugated polymers, Phys. Rev. B **43**, 6781–6784 (1991)
[83] S. V. Frolov, Z. Bao, M. Wohlgenannt, Z. V. Vardeny: Excited-state relaxation in $\pi$-conjugated polymers, Phys. Rev. B **65**, 205209 (2001)
[84] H. Zhao, S. Mazumdar, C.-X. Sheng, M. Tong, Z. V. Vardeny: Photophysics of excitons in quasi-one-dimensional organic semiconductors: Single-walled carbon nanotubes and $\pi$-conjugated polymers, Phys. Rev. B **73**, 075403 (2006)

## Index

density matrix, 325, 336

el–ph scattering, 328
electron-gas thermalization, 327
exciton dynamic, 329, 330
  dissociation, 343
  environmental effect, 333, 334
  exciton–exciton annihilation, 329, 338, 342
  intersubband relaxation, 329, 331
  radiative lifetime, 331, 332
  recombination, 329
  temperature dependence, 334

instrumentation for ultrafast spectroscopy, 322
  pump-probe, 322–324
  streak camera, 324
  time-correlated single photon counting (TCSPC), 324
  upconversion, 324

polarization, 324, 325

TRPE
  time-resolved photoemission, 323